Faraday Discussions
Cite this: DOI: 10.1039/d5fd00160a

PAPER

Coherent sum-frequency generation *via* continuous-wave laser excitation within plasmonic nanogap arrays

Rakesh Arul, †* Caleb Todd, †* Yeeun Roh, Nicolas Spiesshofer, Fiona Bell and Jeremy J. Baumberg

Received 10th December 2025, Accepted 10th February 2026
DOI: 10.1039/d5fd00160a

Mid-infrared (MIR) vibrational spectroscopy offers rich chemical specificity but is limited by detector noise, thermal background, and reliance on high-peak-power or phase-matched nonlinear optics. We show that plasmonic multilayer aggregates (MLaggs), robust, disordered Au nanoparticle films with reproducible nanogaps, enable continuous-wave coherent sum-frequency generation (SFG) between MIR and near-infrared (NIR) light, achieving nonlinear upconversion efficiencies typically associated with ultrafast lasers. Co-localised MIR and NIR confinement produces clear resonant vibrational signatures and a non-resonant plasmonic background. Spatial SFG mapping reveals that MIR and NIR hotspots only partially overlap, showing that their field localisation may be structurally decoupled. Time-resolved measurements confirm that MLaggs preserve ultrafast vibrational coherence. These results unify surface-enhanced IR absorption and Raman spectroscopy (SEIRA/SERS) field enhancement with low-power nonlinear vibrational spectroscopy, removing the need for phase matching and high peak intensities. MLaggs thus provide a path toward compact MIR-to-visible transducers for chemical sensing and integrated photonics.

Introduction

Vibrational spectroscopy is essential to sensing, molecular physics, and metrology, with applications ranging from biomedicine to manufacturing. Mid-infrared (MIR) spectroscopy is especially powerful because the fingerprint region (500–1500 cm^{-1}) enables highly selective molecular identification. However, its practical deployment remains limited by low detector sensitivity, strong thermal backgrounds at room temperature, and the scarcity of inexpensive MIR laser sources. These constraints have driven growing interest in MIR detection through upconversion, which transduces MIR signals into the visible or near-

NanoPhotonics Centre, Cavendish Laboratory, Department of Physics, University of Cambridge, JJ Thompson Avenue, Cambridge, CB3 0US, UK. E-mail: cat64@cam.ac.uk; ra554@cam.ac.uk
† These authors contributed equally.

infrared (NIR), where Si-based detectors operate with high efficiency. This can be performed with incoherent-based approaches, involving heating a material to modulate its optical properties[1,2] or parking excitations in long-lived systems such as lanthanide ions,[3] or coherent approaches involving nonlinear optical media.[4,5] Both approaches often require high-peak-intensity pulsed laser sources to pump the system, especially the coherent nonlinear optical method which also requires delicate and broadband phase matching. This limits the upconversion approach from widespread use.

Recently, plasmonic assemblies which trap light and confine them in ultrasmall mode volumes to achieve large optical field enhancements have been used to enhance the performance of coherent nonlinear optics. The ultrasmall optical mode volumes arise from light confinement in the gaps between plasmonic metal nanoparticle assemblies, which we refer to as nanogaps. This has been shown to enhance second harmonic generation, and even coherent sum-frequency upconversion of MIR and NIR light with continuous-wave low peak power lasers.[6,7] This is a step change for the field of nonlinear optical upconversion and unlocks many opportunities. Typical demonstrations show the upconversion enhancement by single nanostructures, which are frequently hard to fabricate and show variability due to the inherent and unsolved difficulty of controlling interfaces and precise morphologies on the nanometre scale.

Below, we show a new platform using robust, reproducible plasmonic nanoparticle assemblies, which enable high-enhancement SEIRA and SERS. We further repurpose them for enhancing sum-frequency MIR upconversion spectroscopy. These nanoparticle assemblies, termed MLaggs, have been exploited previously for steady-state and *in situ* spectroscopy.[8–10] We now show their utility in enabling coherent nonlinear optics with continuous wave or low peak intensity irradiation due to field enhancement within plasmonic nanogaps.

Results and discussion

MLAgg fabrication and optical properties

Mono- and multi-layer MLAgg films have been established as a reproducible platform for surface-enhanced Raman and IR spectroscopies.[8] The fabrication process is simple and reliable, detailed in the Methods and in Fig. 1a. In brief, colloidal citrate-capped Au nanoparticles (AuNPs) are mixed with an aggregation agent such as cucurbit-5-uril (CB[5]) and shaken to form aggregates of fractal AuNP chains in solution. These chains then settle and concentrate at the interface with chloroform, and excess solutes and citrate can be washed by repeated dilution with deionised water. The remaining aqueous phase is then concentrated to a bead of AuNP aggregates which can be drop-casted and dried on the surface of CaF_2, a mid-infrared transparent substrate, or deposited onto an Au mirror. The resulting film can then be oxygen plasma cleaned to remove contaminant molecules, and re-scaffolded by the molecule of interest – below we study the vibrational probe molecule 4-nitrothiophenol (4-NTP). The re-scaffolding/ReSERS[9,11] process can be performed with oxygen plasma or electrochemically, and its chemical mechanism has recently been elucidated.[12] The re-scaffolding process, involving Au oxides, Au chlorides and the re-establishment of a reproducible nanoscale gap after contaminants are cleaned is crucial to reliable and reproducible nanogap fabrication.

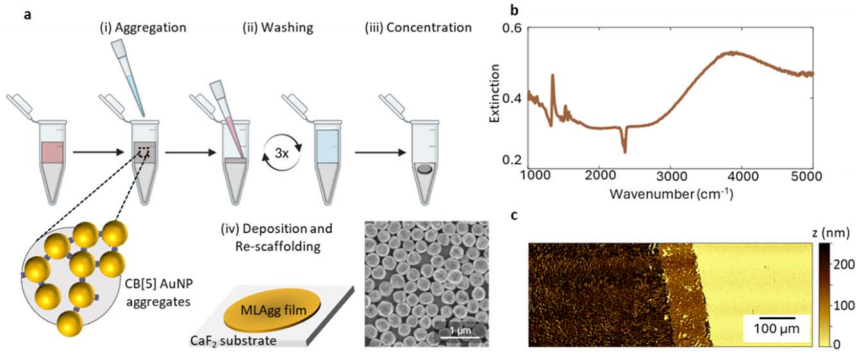

Fig. 1 Plasmonic aggregate films fabrication and optical properties. (a) Synthesis procedure for MLAgg films involving aggregation in solution of gold nanoparticle (AuNP, 250 nm diameter) colloids with cucurbit-5-uril (CB[5]) on an aqueous–chloroform interface, washing with deionised water, and concentration prior to deposition on a mid-infrared transparent CaF_2 substrate. Inset shows an SEM image of the aggregated nanoparticles. (b) MIR extinction spectrum of MLAgg films at the monolayer regions. (c) Optical profilometer image of deposited MLAgg films.

The resulting film has collective plasmonic modes in both the visible and MIR regimes (peaks in Fig. 1b), which have been extensively characterised.[8,13] The visible and near-IR modes are due to localized plasmon resonances, and lie in the 500–800 nm spectral region, and depend on local nanoparticle arrangements and nanogap morphologies.[8,13] The MIR mode is the result of a high effective refractive index in the film and consequent Fabry–Perot resonance.[8,13] The close-packed gold nanoparticle aggregate array acting as a low-loss metamaterial, with a tunable refractive index set by the fill-fraction of gold and dielectric. The refractive index can be tuned to $n > 10$ and controlled by making binary combinatorial metamaterials of Au and Ag nanoparticle arrays.[13]

The MLAgg metamaterial confines MIR light into the thin film, especially the nanogaps, with effective optical mode volume compression factors[8] of 10^{-8}, meaning light in the MIR is squeezed down to around 7 nanogaps, with visible light confined even tighter. Fig. 1b shows the presence of a mode at 2619 nm or 3819 cm^{-1}. Additional SEIRA resonances from the re-scaffolded 4-NTP molecule are present, especially the strong NO_2 stretch vibration at $\nu_{vib} = 1338$ cm^{-1}. The resonance is strongly enhanced, evidenced by the strongly asymmetric Fano lineshape expected from coupling to the plasmonic mode.[8,14]

The as-deposited films have regions of single layers and multi-layers (Fig. 1c) and can be stacked to tune the MIR resonance further out into the far-infrared (>10 μm wavelength).[8] Within such tightly confined nanogaps, the optical field enhancement (E/E_0) in the visible and MIR can be very large, resulting in SEIRA enhancement factors $\sim 10^6$, and a corresponding enhancement in all nonlinear optical processes which rely on the field strength to a higher power.

CW SFG in MLAgg

Nonlinear optical processes arise from an anharmonic polarisation response of the material to an incident electric field. In the linear regime, the polarisation of

a material is related to an incident electric field by $P = \varepsilon_0 \chi E$, but for large electric fields this approximation fails. Instead, we can expand the polarisation as a Taylor series: $P = \varepsilon_0 \chi^{(1)} E + \varepsilon_0 \chi^{(2)} E^2 + \cdots$. Oscillating terms in E (in our case, one at ν_{NIR} and one at ν_{MIR}) are multiplied together, creating terms in P oscillating at the sum ($\nu_{NIR} + \nu_{MIR}$) and difference ($\nu_{NIR} - \nu_{MIR}$) frequencies, which become sources for electric field oscillations at those frequencies (*i.e.* sum- and difference-frequency generation). The frequency conversion efficiency is typically very low but can be enhanced by the presence of a real intermediate energy state such as a molecular vibration.[15–18] In this resonant case, the SFG can be viewed as a MIR photon being absorbed to excite a vibrational state, from which an anti-Stokes Raman scattering event occurs, which we have illustrated in the Fig. 2a inset. From this, it is easy to see that the upconverted power is bilinear in the NIR and MIR powers (in the limit of no depletion):

$$I_{SFG} \propto I_{NIR} I_{MIR}$$

Typically, these processes require ultrafast pulsed lasers with high peak intensities to produce measurable outputs. In plasmonic nanogap systems, however, co-localization and enhancement of the NIR and MIR fields enable nonlinear signals even under continuous wave excitation and low average powers.[6,7,19]

To investigate the potential for MLaggs to act as a MIR upconversion platform, we fabricated a single-deposition (1–2 layers) sample of 250 nm AuNPs aggregated by the molecule 4-NTP, whose NO_2 functional group has a symmetric stretch vibration at 1338 cm^{-1} which is strongly Raman- and MIR-active. The aggregate was deposited onto a CaF_2 substrate which is transparent from the visible through to the MIR. We focused a continuous-wave 785 nm NIR laser onto the sample from above and a tunable continuous-wave MIR laser (set to 1338 cm^{-1}) to the same position from below and collected surface-enhanced Raman scattering (SERS) spectra. In Fig. 2a, we compare a spectrum taken with the MIR off (black

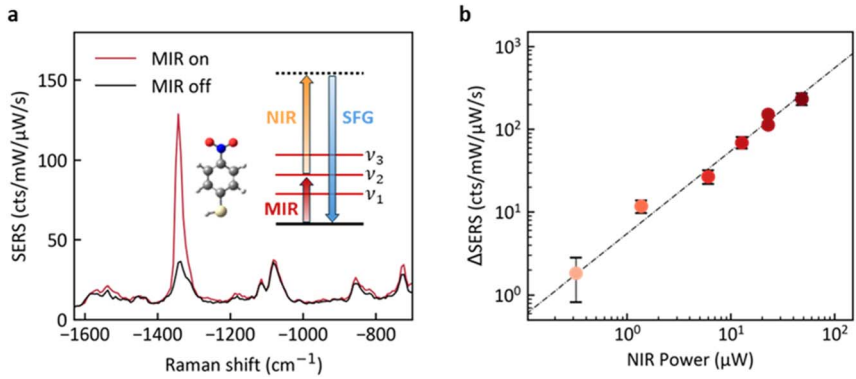

Fig. 2 Sum-frequency generation in plasmonic aggregate films. (a) Comparison between SERS spectra of 4-NTP with and without a 228 μW MIR pump tuned to 1338 cm^{-1} (resonant with the symmetric stretch vibration of the NO_2 functional group), with inset schematic of the vibrationally-enhanced SFG energy levels. (b) Dependence of upconverted counts at 1338 cm^{-1} on 785 nm NIR probe laser power with error bars determined by repeat measurements and a linear fit (dashed line) through the origin.

curve) to one with the MIR on (red curve). The signal is unchanged except for a large increase at the sum-frequency, which is a signature of the coherent (non-thermal) SFG process outlined above. The measured SFG signal depends linearly on the power of the 785 nm NIR beam (Fig. 2b), indicating the SFG is a one-photon process with respect to the NIR, as predicted. This helps to rule out significant influence from bleaching or NIR vibrational pumping/optomechanics.[20]

Next, we conducted a sweep of the MIR wavenumber to observe the background and resonant contributions to upconversion efficiency. The SFG intensity (normalised to MIR pump power) varies as a function of MIR pump frequency and has a resonant response at the NO_2 stretch vibration, seen in Fig. 3a in the 2D plot of MIR pump frequency ν_{MIR} *vs.* anti-Stokes Raman spectrum. The map reveals a strong, vibrationally resonant feature at 1338 cm^{-1}, weaker vibrationally resonant features at *e.g.* 1076 cm^{-1} and 1568 cm^{-1}, and a non-resonant broadband SFG response at almost all MIR pump frequencies (diagonal line in Fig. 3a). The non-resonant SFG originates from the intrinsic $\chi^{(2)}$ nonlinearity of the surface of the Au and the plasmonic system.[21,22]

A line-cut across the wavelength sweep is extracted in Fig. 3b for both the SFG and DFG regions. The DFG response is both weaker than the SFG and significantly noisier. The former relates to the detunings of all involved fields from the upconversion platform's multiple resonances,[23] while the latter is likely due to the larger background (and therefore noise) in spectra on the Stokes side of the NIR pump. There is an asymmetric, Fano-like response to the SFG upconversion at the resonant vibrational modes, which corresponds to an interference between the vibrationally resonant SFG and the background non-resonant SFG. The overall SFG response I_{SFG} can be decomposed[15] into a resonant response modelled by

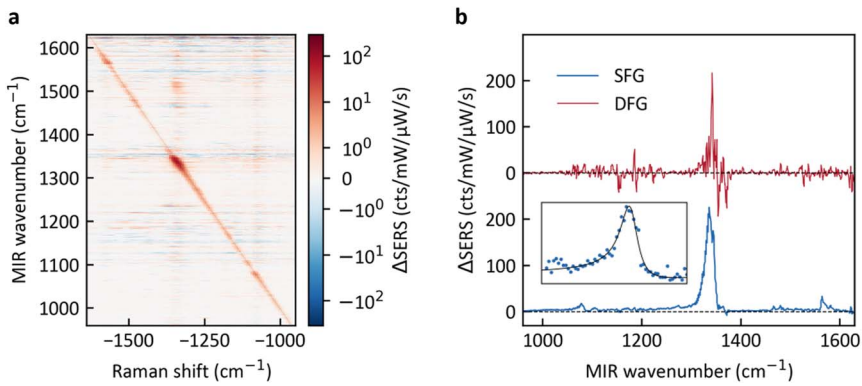

Fig. 3 Mid-infrared wavenumber dependence of sum-frequency generation. (a) Difference spectra (MIR on − MIR off) as the MIR wavenumber is tuned between 960 cm^{-1} and 1630 cm^{-1}, with colour mapped on a log scale (except between ±1 to avoid the singularity at 0) and normalized to the NIR and MIR powers. (b) Difference spectra evaluated at the MIR pump wavenumber on the Stokes (DFG, top red curve) and anti-Stokes (SFG, bottom blue curve) sides of the 785 nm pump, plotted on the same scale and vertically offset for clarity. Inset shows a fit (black) to the main SFG peak at 1338 cm^{-1}, corresponding to interference between resonant and non-resonant contributions to the SFG.

a Lorentzian of amplitude A_{vib}, frequency ν_{vib} and linewidth Γ, and a non-resonant response of amplitude A_{NR} and phase ϕ.

$$I_{SFG} = \left| A_{NR} e^{i\phi} + \frac{A_{vib}}{\nu_{MIR} - \nu_{vib} + i\Gamma} \right|^2$$

Applying this equation to the spectrum in the inset of Fig. 3b, scanned across the NO_2 stretch vibration of 4-NTP, yields a good fit, enabling extraction of the phase $\phi = 129°$, and amplitude ratio of resonant to non-resonant of $A_{vib}/A_{NR} = 37$. This response is broadly consistent with that observed recently by Xie *et al.*,[21] with the identity of the molecule in the nanogap contributing heavily to the ratio of resonant to non-resonant terms, indicating that molecules likely change the intrinsic nonlinear optical constants of the surface of Au *via* chemical interactions.

Spatial dependence of SFG in MLAgg

Now we will elaborate on how spatial inhomogeneity affects SFG in MLaggs. A significant body of plasmonics research is directed towards the contributions and challenges of so-called "hotspots" to surface sensing. The nanoscale details of any plasmonic substrate strongly influence its local electric field environment, creating locations where enhancement factors are enormously larger than elsewhere in the system. Examples include sharp tips,[24] nanometre gaps in a coupled system,[25] or, in the ultimate extreme, "picocavity" adatoms which localise electric fields down to single-molecule scales.[26] Frequently, the vast majority of a substrate's SERS signal comes from a handful of molecules located near these hotspots.[27] As such, significant effort has been expended on locating, activating, creating, or removing spatial inhomogeneities.[27]

In disordered plasmonic assemblies, the (inhomogeneous) local arrangement of nanoparticles causes significant variation from gap to gap in both field enhancement and far-field coupling. This has been shown, for example, in both fractal and non-fractal aggregates.[8,28,29] Understanding these hotspots is especially important to nonlinear optical processes, as the field enhancement of each involved frequency contributes nonlinearly to the overall efficiency. In particular, SFG at the nanoscale requires the MIR and NIR electric fields to be co-localised in space, replacing the requirement for phase matching in bulk nonlinear optics with mode matching.[30]

We can utilize this property to study the localisation characteristics of the MIR field and obtain a "super-resolution" image of the MIR field *via* upconversion with visible/NIR wavelengths.[31] To do so, we conducted a spatial map of SFG signal in a 40 μm × 50 μm region of an MLAgg sample at 2 μm intervals (Fig. 4). We plot the upconverted counts at each position in Fig. 4b and overlay a greyscale dark field microscopy image of the region at 50% transparency (positional uncertainty around 2 μm). First, note that most locations exhibit a similar upconversion strength on the order of 100 cts mW^{-1} μW^{-1} s^{-1}. However, a handful of points significantly exceed this value. Some of these SFG hotspots may be accounted for by the visible/NIR field enhancement: the overlaid darkfield image shows some correlation between strongly visible-light scattering and strongly upconverting locations. However, large SFG signal was also detected in locations which were not strongly scattering, implying a contribution from the MIR field enhancement

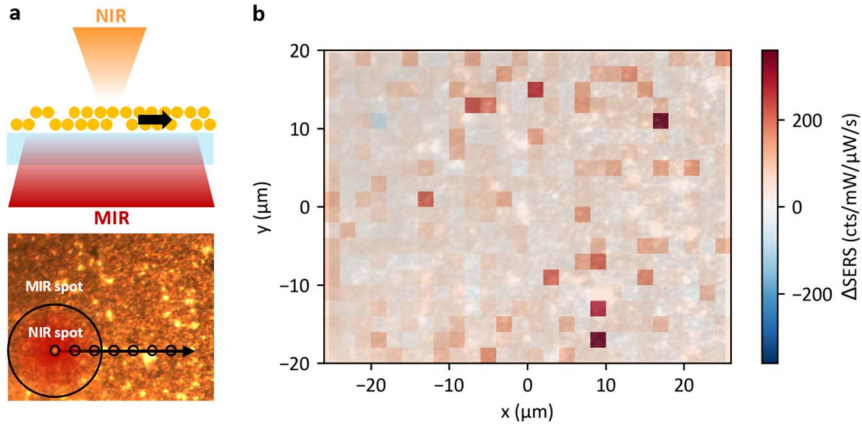

Fig. 4 Spatial map of sum-frequency generation. (a) Schematic showing the spatial mapping procedure (top) and image of the mapped region with approximate NIR/MIR spot sizes and measurement spacings indicated (bottom). (b) Colour map of upconverted counts in a 40 μm × 50 μm grid with 2 μm spacing, overlaid by a greyscale dark field scattering image of the mapped region at 50% transparency. Intensity of signal normalized by the NIR (μW) and MIR pump (mW) powers.

independent of the visible enhancement. Though the MIR and NIR fields are colocalised to some extent in every gap, they are not enhanced directly in proportion to each other in each gap. This is expected, since the two fields are probing structure on different length scales due to their distinct wavelengths, focal sizes, and field localizations on the nanoscale, which we investigate further in the last section.

Time-resolved SFG in MLAgg

We demonstrate the utility of the MLAgg platform to enhance conventional ultrafast pulsed laser excited nonlinear optics as well, thus allowing us to probe the coherence lifetime of the 4-NTP transition. Fig. 5a shows the SFG difference

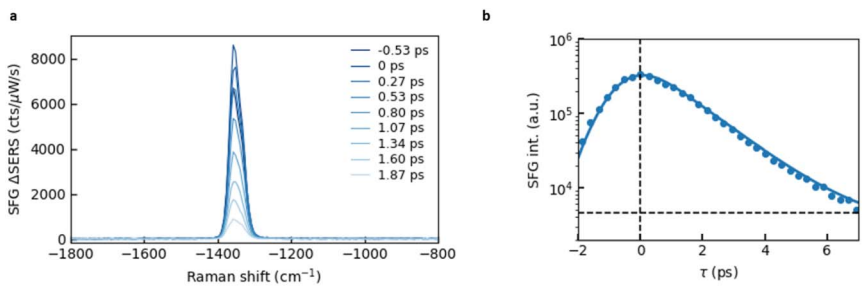

Fig. 5 Ultrafast time-resolved MIR-pump, NIR-probe spectroscopy of 4-NTP vibrations in plasmonic MLaggs. (a) Sum frequency generation spectra (MIR pump at 1338 cm^{-1}, NIR 785 nm probe, 1 ps pulse duration, 80 MHz repetition rate) of 4-NTP in MLAgg assemblies. Background MIR-off anti-Stokes spectrum subtracted. (b) Time-resolved SFG decay *vs.* pump–probe delay.

signal as a function of time delay between the MIR pump and NIR probe. Fitting the vibrational decay lifetime again requires accounting for a resonant and non-resonant contribution to the time decay signal using the molecular dipole response function model below:[15]

$$R_{\mathrm{mol}} = A_{\mathrm{NR}} e^{i\phi_{\mathrm{NR}}} + A_{\mathrm{vib}} e^{-t/\tau_{\mathrm{vib}}} e^{-i(\omega_{\mathrm{vib}} t + \phi_n)}$$

The total time-resolved signal observed is then proportional to the second order polarisation:

$$|P^{(2)}(t,\tau_{\mathrm{vib}})|^2 \propto |E_{\mathrm{NIR}}(t - \tau_{\mathrm{vib}}) \times [E_{\mathrm{MIR}}(t) \times R_{\mathrm{mol}}(t)]|^2$$

We fitted this model to the decay trace measured in Fig. 5b, showing the integrated intensity of SFG as a function of the time delay. The good agreement between the data and model enables the extraction of a vibrational coherence lifetime of $\tau_{\mathrm{vib}} = 2.8$ ps.

Visible and infrared optical modes in disordered AuNP assemblies

The scattering spectrum of 250 nm AuNPs was simulated, using multiple sphere Mie scattering code,[32] for linear chains comprising 1 to 20 nanoparticles with a 0.9 nm gap between nanoparticle surfaces and light polarized along the chain's long axis. AuNPs can couple with each other *via* capacitive coupling due to charge separation between one nanoparticle and another when plasmons are driven by an oscillating electric field. This gives rise to a bonding dipolar plasmon (BDP) between nanoparticles separated by a gap of ~1 nm. The spectrum in Fig. 6a shows the redshift and broadening of the BDP mode as the chain length increases, saturating at a chain length of 10 NPs. The redshift of the mode can be understood as the coupled dipoles oriented along the chain length forming a superradiant mode delocalized across the whole chain. The broadening of the peak is due to the enhancement of non-radiative/absorptive losses as the field is now delocalized over a larger portion of the nanoparticle chain. The mode

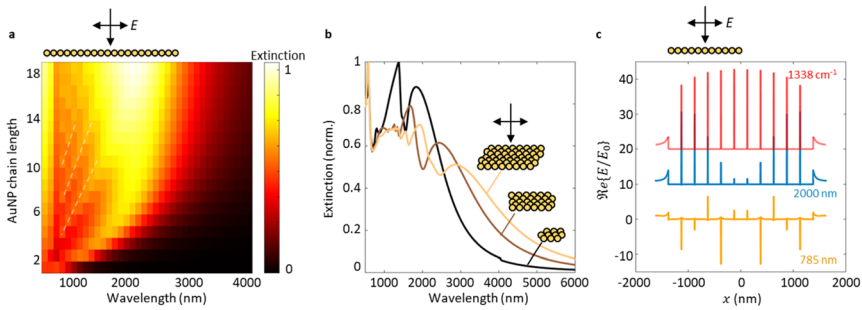

Fig. 6 Optical modes and field confinement in AuNP chains and platelets. (a) Simulated normalized extinction spectrum for varying chain lengths of AuNPs (250 nm diameter) showing formation of collective plasmonic modes. (b) Simulated normalized extinction spectra of platelets of AuNPs of increasing lateral dimension (4 × 3, 5 × 6, 6 × 8) showing redshift of collective mode. (c) Simulated optical field enhancement along the centre of an 11 AuNP chain showing localization of different frequencies in the nanogaps (near-IR: 785 nm, shortwave-IR: 2000 nm, MIR: 4-NTP resonance at 1338 cm^{-1}).

saturates at ~2000 nm, due to the decay length of the plasmon and the extent of coupling setting a limit on the degree of redshift. There are higher order modes corresponding to standing waves of the electric field within the linear chain, of which only the odd-symmetry ones are visible as "bright" modes with a non-zero dipole moment.

To redshift the modes even further, we can extend the nanoparticles beyond two chains and simulate a full extended 2D film. This is challenging to do for nanoparticles unless with periodic boundary conditions in a full-wave simulation. Hence, we simulate platelets of increasing lateral dimension in Fig. 6b, which show a redshift of the mode further out to 3200 nm, which starts to match the experimental FTIR spectrum in Fig. 1b. To account for the lateral confinement differences for MIR and visible light, especially in the presence of disorder, is challenging for full-wave simulations and impossible for effective medium models. We approximate this by looking at the field localization in Fig. 6c, which shows that different wavelengths experience different magnitudes of field enhancement and within different gap locations. The MIR (at 1338 cm^{-1}) is localized like a standing wave between the ends of the chain, and shorter wavelengths look like higher orders of a standing wave within the structure, as observed before.[8,33]

To better understand the characteristics of the plasmonic aggregate films, it is useful to consider them as a metamaterial in the MIR and NIR regimes (possible due to the sub-wavelength scale of the AuNP meta-atoms). It has recently been shown that the collective system displays behaviours distinct from its constituent parts: it can be described as a dielectric with a large effective refractive index ($n >$ 5) that depends on the fill-fraction of plasmonic metal *vs.* dielectric gaps.[13] The MIR modes can be predicted by calculating the expected Fabry–Perot resonances of the equivalent dielectric thin film.

Conclusions

In this work, we demonstrate that plasmonic multilayer aggregates (MLaggs) provide a robust, reproducible, and chemically versatile platform for continuous-wave coherent sum-frequency generation in the MIR, revealing nonlinear upconversion efficiencies typically accessible only with ultrafast lasers. By co-localising and enhancing MIR and NIR fields within disordered yet strongly confining plasmonic nanogaps, MLaggs enable broadband SFG upconversion at $\mu W\ \mu m^{-2}$ intensities, producing clear resonant vibrational signatures alongside non-resonant SFG backgrounds. These results harness the optical confinement properties of plasmonic MLaggs, previously used for surface-enhanced spectroscopies (SEIRA, SERS), to improve nonlinear coherent vibrational spectroscopy. Nonlinear spectroscopy traditionally relies on phase-matching and high-peak-power sources; plasmonic confinement in disordered MLAgg films removes both barriers, enabling table-top, low-power nonlinear vibrational spectroscopy.

Spatial mapping reveals that SFG hotspots only partially correlate with visible-light scattering, highlighting that MIR field localisation may be structurally distinct from NIR localisation. This disentangling of visible and MIR enhancement channels is a key insight for the field: in contrast to conventional SERS hotspots, nonlinear MIR upconversion requires simultaneous confinement of two

disparate wavelengths, which MLaggs achieve through their collective visible and MIR plasmonic modes. This also leads to an intriguing opportunity: the MIR local field distribution can be interrogated at sub-diffraction-limited resolution using the NIR beam, and a more detailed study of spatial SFG correlations could provide rich information on both the MIR mode structure and the nanogap-scale photonic landscape. Time-resolved MIR-pump/NIR-probe SFG further shows that MLaggs enhance ultrafast nonlinear signals without obscuring vibrational coherence, enabling measurement of femtosecond–picosecond decay pathways within highly confined optical volumes. In contrast to recent CW MIR-visible SFG studies based on lithographically defined, single-cavity plasmonic metasurfaces, our MLAgg platform offers broadband MIR resonances, scalability, and chemical reconfigurability *via* re-scaffolding.

Together, these results expand the scope of plasmon-enhanced spectroscopy beyond passive field enhancement toward active MIR frequency conversion, coherent control, and nanoscale vibrational dynamics. Future work will perform correlated SFG mapping to reconstruct MIR mode patterns, engineer multilayer metamaterial MLAgg stacks to access longer wavelength resonances, and integrate MLAgg upconversion with CMOS detectors directly.

Methods and materials

MLAgg fabrication

Disordered AuNP films were formed by adding 500 μL of gold nanoparticles (250 nm diameter, citrate capped, BBI Solutions) to 500 μL of chloroform in an Eppendorf tube. Aggregation was initiated by the addition of 150 μL of CB[5] (cucurbituril-5-hydrate, Sigma Aldrich), followed by immediate vigorous shaking for 1 minute. After shaking, the solution was left to settle for another minute, causing the separation of the immiscible chloroform and aqueous phases. The aggregated gold nanoparticles then settled to the interface between the two phases. The aqueous phase was thrice washed by the addition and removal of 500 μL of water to dilute the citrate salts. The aqueous phase was then slowly concentrated by removal of water till a dense Au aggregate bead was formed in the chloroform phase. The bead was then deposited onto a calcium fluoride substrate (Crystran). After drying overnight, the MLaggs were treated with O_2 plasma for 40 minutes to form oxidation between the nanoparticles. They were then immersed in a 1 mM 4-NTP solution for 10 minutes and subsequently rinsed with water. The MLAgg films were then characterized with an FTIR microscope (Shimadzu AIM-9000 FTIR microscope, liquid nitrogen cooled MCT detector, Cassegrain 15× objective 0.7 NA, 20 μm spot size, Happ–Genzel apodization) and with a white light vertical scanning profilometer (Bruker Contour GTK).

SFG microscopy

A tunable QCL MIR pump laser (LaserTune, Block Ltd) operating at a 5% duty cycle was focused onto the sample from below through a 0.5 NA 40× reflective objective (Thorlabs). A 785 nm diode laser (MatchBox, Integrated Optics Ltd) was passed through an AOM operating at a 15% duty cycle synchronised to the QCL to temporally overlap the MIR and NIR pumps, before being focused onto the sample from above through a 0.9 NA 100× dark field objective in a customised

commercial microscope (BX51, Olympus). Light was collected in reflectance and sent through notch filters (785-20 NNF, Iridian) to remove Rayleigh scattered light. The remaining light was passed through a monochromator (i303, Shamrock) and dispersed by a 150 lines per mm grating onto an EMCCD (Newton, Andor).

Time-resolved SFG microscopy

A pump laser (APE Emerald Engine: repetition rate 80 MHz, pulse duration 2 ps) simultaneously drives two commercial optical parameter oscillators (Levante IR ps, APE): one feeding a DFG (HarmoniXX DFG, APE) and the other feeding a SHG (HarmoniXX THG, APE). The DFG system produces MIR pulses ($\lambda_{MIR} = 7.46$ μm), while the SHG system generates visible pulses at 785 nm. Both the visible and MIR beams are incident into a custom-built microscope and focused using a dark-field objective (0.9 NA, 100×, Olympus) and a reflective Cassegrain objective (0.8 NA, 100×, Pike). The spectra are dispersed by 150 lines per mm grating (Kymera 328i, Andor) and detected by an EMCCD camera (Newton 920, Andor).

Conflicts of interest

The authors declare no competing financial interest.

Data availability

The datasets generated during and/or analysed during the current study are available from the authors on reasonable request. The files used for simulations are also available upon reasonable request.

References

1 Q. Xia, J. Yin, Z. Guo and J.-X. Cheng, Mid-infrared photothermal microscopy: principle, instrumentation, and applications, *J. Phys. Chem. B*, 2022, **126**, 8597–8613.
2 Y. Zhang, *et al.*, Fluorescence-detected mid-infrared photothermal microscopy, *J. Am. Chem. Soc.*, 2021, **143**, 11490–11499.
3 L. Liang, C. Wang, J. Chen, Q. J. Wang and X. Liu, Incoherent broadband mid-infrared detection with lanthanide nanotransducers, *Nat. Photonics*, 2022, **16**, 712–717.
4 K. Huang, J. Fang, M. Yan, E. Wu and H. Zeng, Wide-field mid-infrared single-photon upconversion imaging, *Nat. Commun.*, 2022, **13**, 1077.
5 R. Arul, *et al.*, Efficient short-wave infrared upconversion by self-sensitized holmium-doped nanoparticles, *arXiv*, 2024, preprint, arXiv:2411.19949, DOI: 10.48550/arXiv.2411.19949.
6 W. Chen, *et al.*, Continuous-wave frequency upconversion with a molecular optomechanical nanocavity, *Science*, 2021, **374**, 1264–1267.
7 A. Xomalis, *et al.*, Detecting mid-infrared light by molecular frequency upconversion in dual-wavelength nanoantennas, *Science*, 2021, **374**, 1268–1271.

8 R. Arul, *et al.*, Giant mid-IR resonant coupling to molecular vibrations in sub-nm gaps of plasmonic multilayer metafilms, *Light: Sci. Appl.*, 2022, **11**, 281.
9 D.-B. Grys, *et al.*, Controlling Atomic-Scale Restructuring and Cleaning of Gold Nanogap Multilayers for Surface-Enhanced Raman Scattering Sensing, *ACS Sens.*, 2023, **8**, 2879–2888.
10 M. Niihori, *et al.*, SERS sensing of dopamine with Fe (III)-sensitized nanogaps in recleanable AuNP monolayer films, *Small*, 2023, **19**, 2302531.
11 S. M. Sibug-Torres, *et al.*, In situ electrochemical regeneration of nanogap hotspots for continuously reusable ultrathin SERS sensors, *Nat. Commun.*, 2024, **15**, 2022.
12 S. M. Sibug-Torres, *et al.*, Transient Au–Cl adlayers modulate the surface chemistry of gold nanoparticles during redox reactions, *Nat. Chem.*, 2025, **18**, 294–301.
13 N. Spiesshofer, *et al.*, Tailoring ultrahigh index plasmonic combinatorial metamaterials for SEIRA and SERS by tuning the fill fraction, *Optica*, 2025, **12**, 1357–1366.
14 N. S. Mueller, *et al.*, Surface-Enhanced Raman Scattering and Surface-Enhanced Infrared Absorption by Plasmon Polaritons in Three-Dimensional Nanoparticle Supercrystals, *ACS Nano*, 2021, **15**, 5523–5533.
15 F. Bell, *et al.*, Coherent Dynamics of Molecular Vibrations in Single Plasmonic Nanogaps, *Phys. Rev. Lett.*, 2025, **135**, 076901.
16 X. Zheng, J. Tan, Q. Pei, Y. Luo and S. Ye, Single-molecule-level detection of interfacial molecular structures and ultrafast dynamics, *Chem. Sci.*, 2025, **16**, 5275–5282.
17 M. Linke, J. Multhaup and E. Hasselbrink, Response of a 4-nitrothiophenol monolayer to rapid heating studied by vibrational sum frequency spectroscopy, *J. Chem. Phys.*, 2024, **161**, 194711.
18 Z. Yu and R. R. Frontiera, Intermolecular forces dictate vibrational energy transfer in plasmonic–molecule systems, *ACS Nano*, 2021, **16**, 847–854.
19 R. Chikkaraddy, R. Arul, L. A. Jakob and J. J. Baumberg, Single-molecule mid-infrared spectroscopy and detection through vibrationally assisted luminescence, *Nat. Photonics*, 2023, **17**, 865–871.
20 L. A. Jakob, *et al.*, Optomechanical Pumping of Collective Molecular Vibrations in Plasmonic Nanocavities, *ACS Nano*, 2025, **19**, 10977–10988.
21 Z. Xie, N. Oyamada, F. Ciccarello, W. Chen and C. Galland, Continuous-wave, high-resolution, ultra-broadband mid-infrared nonlinear spectroscopy with tunable plasmonic nanocavities, *arXiv*, 2025, preprint, arXiv:2508.12097, DOI: 10.48550/arXiv.2508.12097.
22 A. Sakurai, *et al.*, Phase-sensitive tip-enhanced sum frequency generation spectroscopy using temporally asymmetric pulse for detecting weak vibrational signals, *arXiv*, 2025, preprint, arXiv:2511.04965, DOI: 10.48550/arXiv.2511.04965.
23 F. Zou, L. Du, Y. Li and H. Dong, Amplifying frequency up-converted infrared signals with a molecular optomechanical cavity, *Phys. Rev. Lett.*, 2024, **132**, 153602.
24 T. Kumagai, K. Miwa and B. Cirera, Point-Contact Tip-Enhanced Raman Spectroscopy: Picoscale Light–Matter Interactions within Plasmonic Cavities, *Nano Lett.*, 2025, **25**, 15449–15459.

25 J. J. Baumberg, J. Aizpurua, M. H. Mikkelsen and D. R. Smith, Extreme nanophotonics from ultrathin metallic gaps, *Nat. Mater.*, 2019, **18**, 668–678.
26 J. J. Baumberg, Picocavities: a Primer, *Nano Lett.*, 2022, **22**, 5859–5865.
27 P. Kerner, R. Arul, D. Thompson, J. J. Baumberg and B. de Nijs, Optical control of single-atom dynamics in plasmonic nanogaps, *Sci. Adv.*, 2025, **11**, eadx3216.
28 C. Carnegie, *et al.*, Mapping SERS in CB: Au plasmonic nanoaggregates, *ACS Photonics*, 2017, **4**, 2681–2686.
29 M. I. Stockman, S. V. Faleev and D. J. Bergman, Localization *versus* delocalization of surface plasmons in nanosystems: can one state have both characteristics?, *Phys. Rev. Lett.*, 2001, **87**, 167401.
30 G.-C. Li, *et al.*, Light-induced symmetry breaking for enhancing second-harmonic generation from an ultrathin plasmonic nanocavity, *Nat. Commun.*, 2021, **12**, 4326.
31 R. Niemann, *et al.*, Spectroscopic and interferometric sum-frequency imaging of strongly coupled phonon polaritons in SiC metasurfaces, *Adv. Mater.*, 2024, **36**, 2312507.
32 D. Mackowski and M. Mishchenko, A multiple sphere T-matrix Fortran code for use on parallel computer clusters, *J. Quant. Spectrosc. Radiat. Transfer*, 2011, **112**, 2182–2192.
33 R. Esteban, R. W. Taylor, J. J. Baumberg and J. Aizpurua, How chain plasmons govern the optical response in strongly interacting self-assembled metallic clusters of nanoparticles, *Langmuir*, 2012, **28**, 8881–8890.